Capturing Secchi disk depth by using Sentinel-2 MSI imagery in Jiaozhou Bay, China from 2017 to 2021

Lei Yang [a], Dingfeng Yu [a,b,*], Huiping Yao [c], Hao Gao [a], Yan Zhou [a], Yingying Gai [a], Xiaoyan Liu [a], Maosheng Zhou [a], Shunqi Pan [b]

[a] Institute of Oceangrahic Instrumentation, Qilu University of Technology (Shandong Academy of Sciences), Qingdao 266100, China
[b] Hydro-Environmental Research Centre, School of Engineering, Cardiff University, Cardiff CF24 3AA, UK
[c] College of Oceanography and Space Informatics, China University of Petroleum, Qingdao 266580, China

A B S T R A C T

Water clarity is a key parameter for assessing changes of aquatic environment. Coastal waters are complex and variable, remote sensing of water clarity for it is often limited by low spatial resolution. The Sentinel-2 Multi-Spectral Instrument (MSI) imagery with a resolution of up to 10 m are employed to solve the problem from 2017 to 2021. Distribution and characteristics of Secchi disk depth (SDD) in Jiaozhou Bay (JZB) are analyzed. Subtle changes in localized small areas are discovered, and main factors affecting the changes are explored. Among natural factors, precipitation and wind play dominant roles in variation in SDD. Human activities have a significant influence on transparency, among which fishery farming has the greatest impact. This is clearly evidenced by the significant improvement of SDD in JZB due to the sharp decrease in human activities caused by coronavirus disease 2019 (COVID-19).

1. Introduction

Secchi disk depth (SDD) is one of the basic parameters to describe the optical properties of water body, which characterizes the transmission, transmittance, reflection, and attenuation of light in water body. It can reflect the water quality, and evaluate the turbidity and eutrophication, hence serving as an important parameter in water quality monitoring (Lee et al., 2015; Pitarch, 2020; Zhang et al., 2021a). The variation in SDD directly reflects the change of water ecological environment, which plays a guiding role in the development of maritime defense shipping, coastal ports and other related social economy (Rohan et al., 2021; Shang et al., 2016). Transparency measurements are usually obtained by the Secchi disk method, which has a history of nearly 160 years (Song et al., 2022; Tyler, 1968; Wernand, 2010). However, although the Secchi disk method is simple to measure transparency and can obtain accurate and effective transparency data, its measurement process is greatly affected by natural weather and human factors. Besides, due to small amount of data obtained and poor spatial-temporal continuity of data, it is unable to realize real-time synchronous monitoring of large areas of water (Liu et al., 2020; Yin et al., 2021a). Compared with the Secchi disk method, remote sensing technology has the advantages of low

measurement cost, large amount of data, wide monitoring range, high collection efficiency, and periodic dynamic coating cover (An et al., 2022). It can realize the monitoring of the areas difficult for the experimental personnel to reach, making up for the defects of the Secchi disk method (Yin et al., 2021b; Zhou et al., 2021). Therefore, remote sensing technology is gradually becoming one of the effective and important means of water transparency monitoring. In recent years, more and more scholars in China and abroad have applied it to the study of water transparency (Li et al., 2018; Liu et al., 2021; Luo et al., 2020; Majozi et al., 2014; Yu et al., 2021). Kabiri (2022) had used Moderate Resolution Imaging Spectroradiometer (MODIS) satellite data to invert the water transparency in the Persian Gulf, Strait Hormuz and the northern Oman Bay, and analyzed the seasonal changes of water transparency in the sea area. He et al. (2017) proposed a semi-analytical algorithm based on the Sea-viewing Wide Field-of-view Sensor (SeaWiFS) satellite data to analyze global ocean transparency monthly from 1997 to 2010 and determine the climate distribution and variation range of global ocean transparency. Zolfaghari and Duguay (2016) applied the linear mixed effect model to the atmospheric correction of the Medium Resolution Imaging Spectrometer (MERIS) reflectance and inverted the temporal and spatial distribution of transparency in Lake Erie from 2004 to 2012.

Mao et al. (2018) analyzed the diurnal and monthly changes of SDD in the Bohai Sea and the Yellow Sea by the Geostationary Ocean Color Imager (GOCI) satellite imagery, finding that the diurnal variation of transparency first increased and then decreased, and that the seasonal variation was high in summer and low in winter. Doron et al. (2011) proposed a semi-analytical algorithm for transparency remote sensing inversion based on MERIS, MODIS and SeaWiFS sensor data.

As the transitional water connecting the ocean and land, nearshore Case II waters often contain diverse natural landscapes such as estuary, wetland, mudflat and beach, forming an important part of the earth's ecological environment (Wang et al., 2021). The changes of various natural landscapes in the waters directly reflect the changes of the ecological environment in the region (Sent et al., 2021). Therefore, monitoring the change of nearshore water transparency is of great significance for guiding coastal aquaculture, nearshore engineering construction and ecological environment protection. Compared with Case I waters in the ocean, nearshore Case II waters have many subtle changes, with ecological environment more significantly affected by natural and human factors. They have the characteristics of complex biological optical properties and fast changes (Zhou et al., 2022). The construction of ship navigation, oil spill and bridge facilities will cause short-term linear and surface mutations in SDD (Dong et al., 2022). However, the satellites with low spatial resolutions such as MODIS, MERIS, SeaWiFS and GOCI cannot monitor the subtle variation in SDD, and cannot achieve the high spatial resolution requirements for the transparency monitoring of Case II waters. The spatial resolution of Sentinel-2 Multi-Spectral Instrument (MSI) imagery is as high as 10 m. There are many studies on the transparency of lakes and reservoirs using Sentinel-2 satellite data. Maciel et al. (2021) used the Sentinel-2 MSI images to analyze the changes in the transparency distribution of lakes and reservoirs in Brazil by machine learning. Qing et al. (2021) proposed an improved semi-analytical model based on the quasi-analytical algorithm (QAA) algorithm and applied it to Sentinel-2 satellite data to improve the remote sensing inversion of transparency of complex inland waters. Sivakumar et al. (2022) inversed transparency changes in the Vembanad lake from Sentinel-2 satellite data and analyzed sources of pollution in the lake.

However, there are few studies on long-time remote sensing inversion monitoring of offshore water transparency. The subtle changes of SDD of nearshore Case II waters are unknown in localized small areas, the factors that affect their changes are unknown, and the impact of coronavirus disease 2019 (COVID-19) on SDD is unknown.

The purpose of our study was three-fold: (1) To discover and reveal subtle changes of SDD of nearshore Case II waters in localized small areas; (2) to analyze the factors that affect these subtle changes of SDD; (3) to study and discuss the impact of COVID-19 on the SDD of nearshore Case II waters.

Therefore, Jiaozhou Bay (JZB) off the southern coast of Jiaodong Peninsula in northern China is taken as the research area in this paper, with the Sentinel-2 dual-satellite operational observation from 2017 to 2021 as the research period. The following studies are carried out: (1) Analyzing the performance of the proposed transparency inversion algorithm model of Sentinel-2 MSI images in JZB; (2) Applying the proposed algorithm to Sentinel-2 MSI images; (3) Analyzing the temporal and spatial distribution characteristics of SDD in JZB and the subtle changes in localized small areas; (4) Analyzing the natural factors and human factors that affect the change of transparency distribution.

2. Materials and methods

2.1. Study area

JZB is located at 35°38'-36°18'N, 120°04'-120°23'E and lies on the southern coast of Jiaodong Peninsula. As is shown in Fig. 1, its total area is about 390 km^2 (Wang et al., 2021; Yuan et al., 2021). Generally , JZB is a fan-shaped semi-closed bay. With a width of about 3 km, the bay mouth is bounded eastward by the southern end of Tuandao and the northern end of Xuejiadao. It relates to the Yellow Sea with the coastline in the bay of about 163 km long, among which the proportion of artificial coastline is up to 85 % (Cai et al., 2022). The water depth in JZB is generally shallow in the north and deep in the south. The average water depth is 6–7 m, and most waters are no >5 m. The rivers into the Bay area are rain-source rivers, mainly including Dagu River, Baisha River,
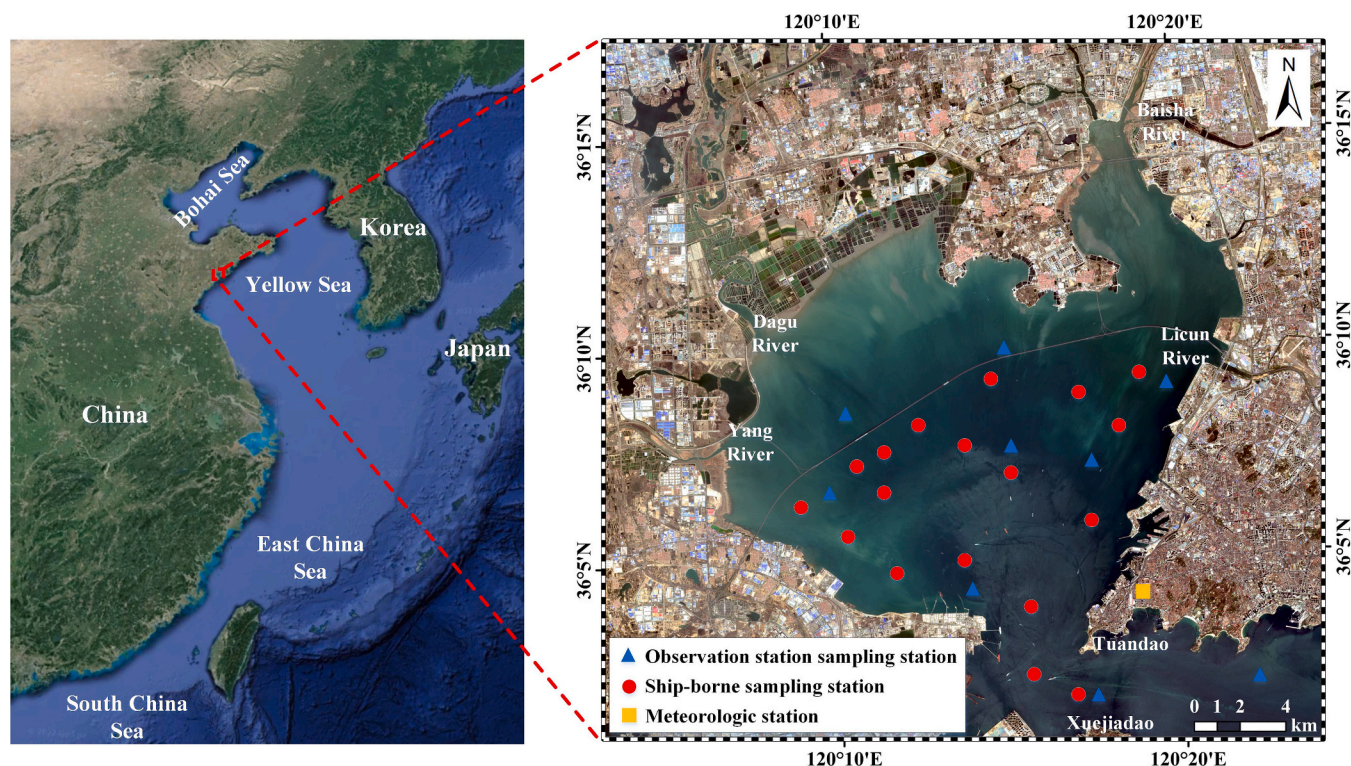

Fig. 1. The location of JZB with all sampling stations and meteorologic station.

Yang River, Licun River and so on (Yu et al., 2022). Affected by the warm temperate monsoon climate, there is no severe cold and summer in the area. The southeasterly wind prevails in summer and the northwesterly wind prevails in winter. The rainfall is mainly concentrated in July, August and September. The tide in the Bay area is a typical half-day tide, with an average tidal difference of 2.71 m and a maximum tidal difference of 6.87 m (Shan and Li, 2020). Here is located Qingdao Port, the fourth largest port in the world in cargo throughput, together with many small fishing boat ports.

In recent years, with the development of social economy near the Bay area, JZB is more and more seriously affected by marine aquaculture, port development, ship navigation, coastal sewage discharge, engineering construction and other human activities. The intensification of human activities continues to increase the pressure on the ecological environment in the Bay area (Yu et al., 2022). As an important indicator of water quality monitoring, transparency reflects the change of water ecological environment; in addition, its distribution characteristics can provide important guiding significance for the distribution of water mass in the sea area, port construction, ship navigation, fishery breeding and ecological environment protection as well as development planning.

2.2. Data

2.2.1. In situ data

The in situ data of transparency in JZB used in this paper are mainly obtained by ship-borne field scientific experiments and fixed observation stations. The ship-borne field scientific experiments mainly include two voyages on November 2, 2016 and May 6, 2017, both with sunny and cloudless weather on the day of the sampling experiments. The on-site transparency measurement method is the Secchi disk method. The number of observation locations in the two ship-borne experiments is 16 and 18, respectively, as is shown in Fig. 1. The measured transparency data of Jiaozhou Bay Observatory are obtained through the National Field Scientific Observation and Research Station of Jiaozhou Bay Marine Ecosystem in Shandong Province (http://jzb.cern.ac.cn/). In total, there are 13 fixed observation stations and 44 measured transparency data is obtained. The measured transparency time of the observatory is mainly distributed in March, June, September and December 2018. The temporal distribution of transparency field measured data is shown in Table 1.

2.2.2. Sentinel-2 MSI data

Sentinel-2 is a high-resolution multispectral imaging satellite, carrying a Multi-Spectral Instrument (MSI) with a height of 786 km and a swath width of 290 km. The ground pixel resolutions are 10 m, 20 m and 60 m, respectively. Sentinel-2 is divided into 2A and 2B satellites for land monitoring, providing images of vegetation, soil and water cover, inland waterways and coastal areas (Main-Korn et al., 2015). Sentinel-2A was launched on June 23, 2015 and Sentinel-2B on March 7, 2017. The revisit cycle of each satellite is 10 days. The two satellites are complementary, and the revisit cycle is 5 days (Su et al., 2018).

Table 1
Information of transparency measured.

Measurement method	Measurement time	Number of transparency measured stations
Ship-borne sample	2016.11.02	16
	2017.05.06	18
Observation station sample	2018.03.09	6
	2018.03.12	5
	2018.06.13	7
	2018.06.20	4
	2018.09.12	8
	2018.09.13	3
	2018.12.12	6
	2018.12.13	2
	2018.12.14	3

All satellite images over JZB since Sentinel-2 operational observation in 2017 were selected as remote sensing data in this paper. A total of 97 images of original L1C level data were downloaded. Sentinel-2 L1C level data are geometric corrected orthophoto data without radiometric calibration and atmospheric correction. In this study, Sen2cor, the atmospheric correction method of Sentinel-2 MSI image provided by ESA, is used for radiometric calibration and atmospheric correction of L1C level data to obtain L2A level data (Su et al., 2018). The L2A-level data after atmospheric correction were preliminarily screened, and the images occluded by clouds were removed to obtain 89 L2A images. The Sentinel-2 MSI imagery cannot be directly processed because of different spatial resolution of each band. Therefore, Sen2Res was used for super-resolution resampling of images, and the band data with spatial resolutions of 20 m and 60 m were resampled to 10 m. ENVI was used to synthesize and analyze the data of each band, and the synthetic data of each image were screened. Finally, 70 images were applied to the transparency model inversion. The process of Sentinel-2 MSI imagery processing is shown in Fig. 2.

The seasonal distribution of the original images, preliminary selected and final images downloaded from 2017 to 2021 are shown in Fig. 3.

2.2.3. Meteorological and hydrological data

The meteorological and hydrological data used in this paper are monthly precipitation, monthly average wind velocity of 10 min, monthly temperature and daily hourly wind velocity, temperature and precipitation downloaded from the National Field Science Observation and Research Station of Jiaozhou Bay Marine Ecosystem (http://jzb.cern.ac.cn/) and National Marine Science Data Center (http://mds.nmdis.org.cn/pages/home.html). The time range is from 2017 to 2021.

2.3. Algorithm

Band ratio method is commonly used for water quality parameter inversion, which can correct the influence of environmental background such as light and atmosphere on the measurement results by comparing the reflectivity of two bands (Chusnah and Chu, 2022; Shang et al., 2011). Based on Sentinel-2 remote sensing reflectance and 16 sets of in situ transparency data in JZB on November 2, 2016, the correlation between band ratios of different bands and transparency data was studied in *Remote sensing retrieval of secchi disk depth in Jiaozhou Bay using Sentinel-2 MSI image* (Yang et al., 2021). Considering the performance of different band ratio algorithm models and the contribution of different band data of Sentinel-2 in nearshore Case II waters, The band ratio empirical algorithm model constructed by the Sentinel-2 MSI imagery of coastal aerosol band (B1, 433–453 mm), blue light band (B2, 458–523 mm), green light band (B3, 543–578 mm) and red light band (B4, 650–680 mm) is used to invert the water clarity in JZB. The algorithm model is as follows

$$f_{SDD}(x) = -5.838 \times x + 1.101 \tag{1}$$

where, $f_{SDD}(x)$ is the water clarity of JZB, and x is the product of band combination logarithm of Sentinel-2 which can be expressed as

$$x = log\left(\frac{B4}{B1}\right) \times log\left(\frac{B4}{B2}\right) \times log(B3 \times B4) \tag{2}$$

2.4. Statistical indicators

In order to evaluate the precision of the transparency retrieval algorithm model and the consistency between the measured transparency data and the inversion data, five indicators, namely, determination coefficient (R^2), root mean square error (RMSE), deviation error (BIAS), unbiased root mean square error (URMSE), absolute error (APD) and relative error (RPD), are used for evaluation. Root mean square error, deviation error and absolute error are used to evaluate the precision of the matching between the inversion data and the measured data.
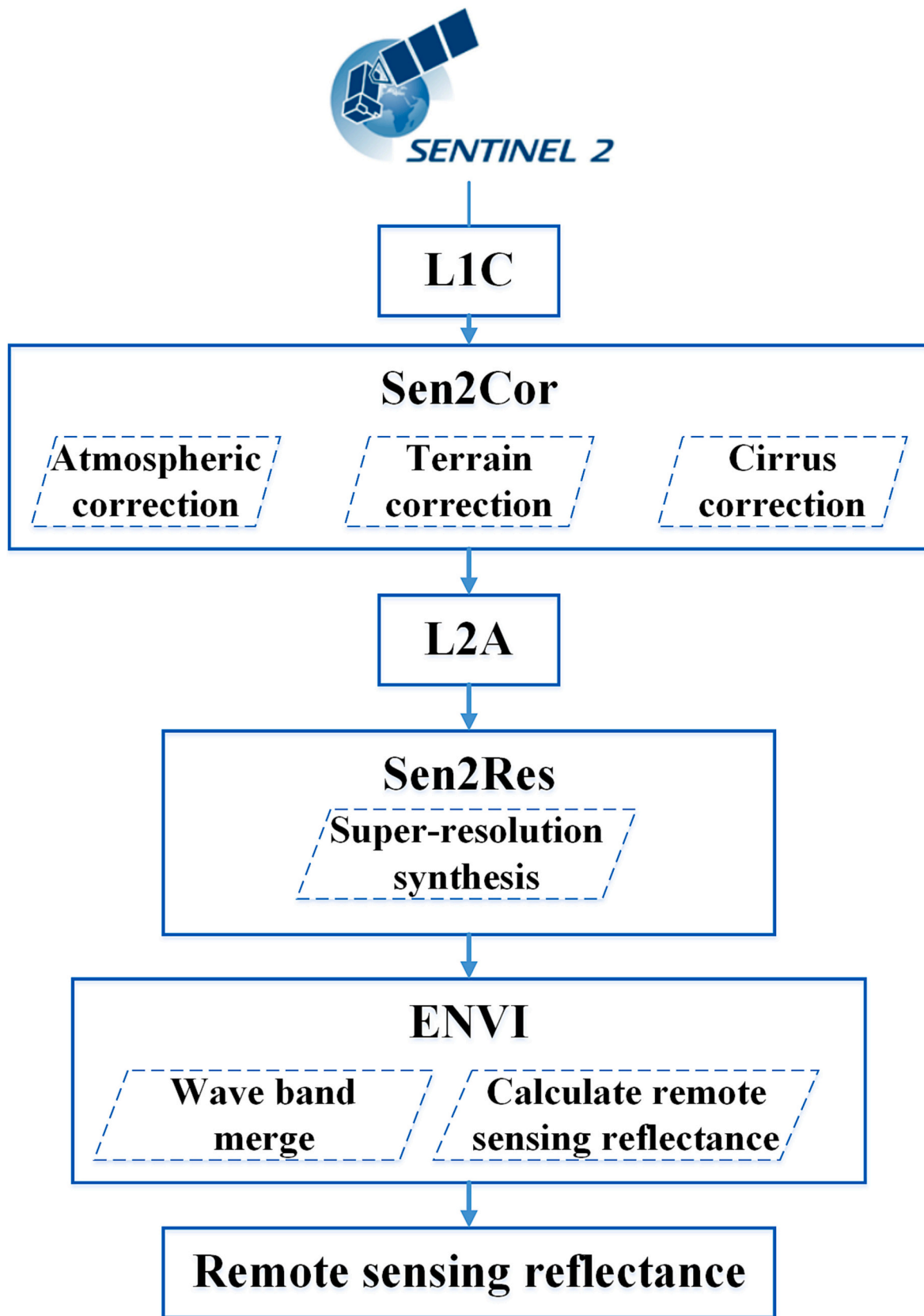
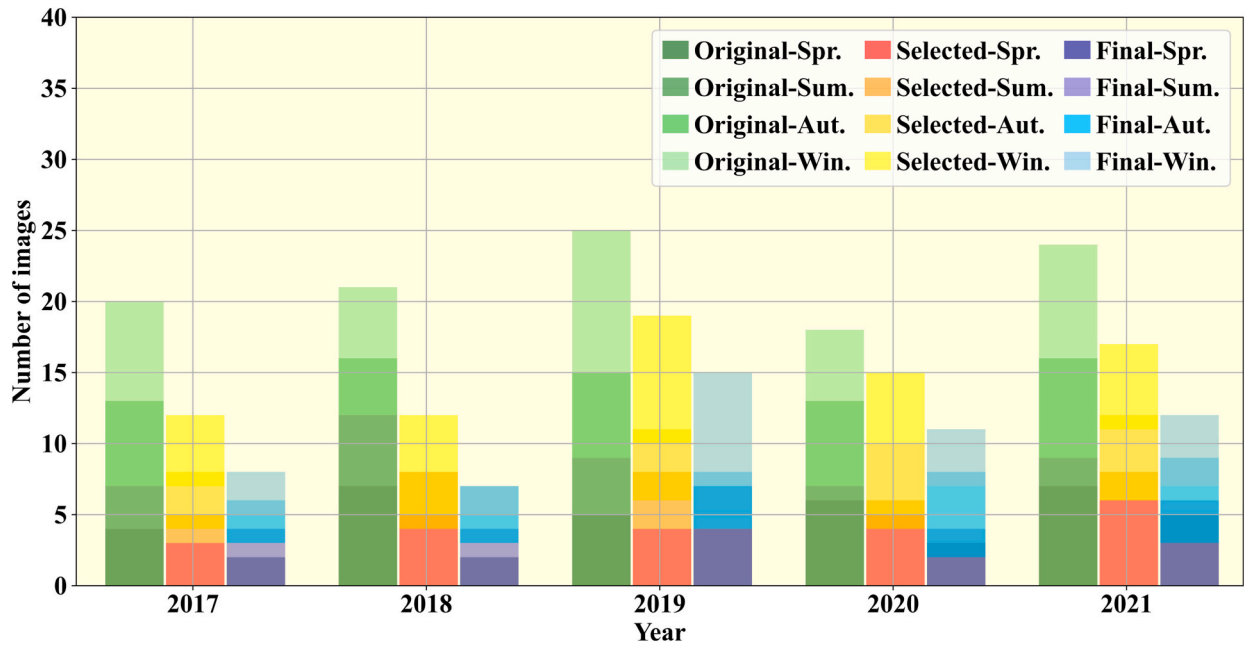**Fig. 2.** The processing flow of Sentinel-2 MSI image.

Fig. 3. The seasonal distribution of original images, selected images and final images from 2017 to 2021.

Relative error is system error index.

$$R^2 = \frac{\sum_{i=i}^{N}(Sate_i - \delta_{onsite})}{\sum_{i=i}^{N}(Onsite_i - \delta_{onsite})} \tag{3}$$

$$R_{BIAS} = \frac{1}{N}\sum_{i=1}^{N}(Sate_i - Onsite_i) \tag{4}$$

$$R_{RPD}(\%) = \frac{1}{N}\sum_{i=1}^{N}\frac{Sate_i - Onsite_i}{Onsite_i} \times 100 \tag{5}$$

$$R_{APD}(\%) = \frac{1}{N}\sum_{i=1}^{N}\frac{|Sate_i - Onsite_i|}{Onsite_i} \times 100 \tag{6}$$

$$R_{RMSE} = \sqrt{\frac{\sum_{i=1}^{N}(Sate_i - Onsite_i)^2}{N}} \tag{7}$$

$$R_{URMS} = \sqrt{\frac{1}{N}\sum_{i=1}^{N}[(Sate_i - \delta_{sate}) - (Onsite_i - \delta_{onsite})]^2} \tag{8}$$

where, *Sate* is the inversion transparency value of satellite data, *Onsite* is the measured transparency value, and *N* is the total number of sampling points, $\delta_{sate} = \frac{1}{N}\sum_{i=1}^{N}Sate_i$, $\delta_{onsite} = \frac{1}{N}\sum_{i=1}^{N}Onsite_i$.

In order to analyze the correlation between SDD and its influencing factors, coefficient and significance test are used for evaluation.

$$r_{x_1x_2} = \frac{\sum(x_1 - \bar{x}_1)(x_2 - \bar{x}_2)}{\sqrt{\sum(x_1 - \bar{x}_1)^2 \sum(x_2 - \bar{x}_2)^2}} \tag{9}$$

$$t = \frac{(\bar{x}_1 - \bar{x}_2) - (\mu_1 - \mu_2)}{\sqrt{\frac{S_1^2}{n_1} + \frac{S_2^2}{n_2}}} \sim t(df) \tag{10}$$

$$df = \frac{\left(\frac{S_1^2}{n_1} + \frac{S_2^2}{n_2}\right)^2}{\frac{\left(\frac{S_1^2}{n_1}\right)^2}{n_1 - 1} + \frac{\left(\frac{S_2^2}{n_2}\right)^2}{n_2 - 1}} \tag{11}$$

where, x_1 and x_2 represent two variables, $\bar{x}_1$ and $\bar{x}_2$ are their sample mean, μ_1 and μ_2 are their population mean, S_1 and S_2 are their sample standard deviation. $n_1 - 1$ and $n_2 - 1$ are their degrees of freedom in the *t*-test.

3. Results

3.1. Calibration and validation of SDD algorithm

Due to meteorological conditions and the 5-day revisiting period of sentinel-2 satellite observations, the imaging time of valid satellite images does not match well with the sampling time of in situ data. However, He et al. (2022) and Zhang et al. (2021b) proposed that in situ data sampling within 7 days of effective satellite imaging time can ensure the effectiveness of the algorithm model. Kloiber et al. (2002) also proposed that the time window between in situ data collection and satellite imaging can obtain reasonable results within 7 days. Olmanson et al. (2008) found that when the time difference between in situ data and satellite imaging increases, the algorithm model does not change significantly. Data with a long-time interval with satellite imaging do not reduce the accuracy of the algorithm model, but only have a small impact on its correlation. Therefore, in order to ensure the effectiveness and accuracy of the algorithm model, a dataset with a time interval of 7 days between in situ data and valid satellite images was selected to evaluate the performance of the algorithm model. Considering the acquisition time of in situ data in Table 1 and the acquisition time of effective Sentinel-2 satellite images, the in situ data of 22 observation stations on March 9, March 12, September 12, and September 13, 2018 met the requirements. However, one observation station on March 9 was not located in our study area, so was March 12, and two observation stations on September 13 were not in our study area. Therefore, we selected a total of 18 groups of data to analyze the performance of the algorithm. The results are shown in Fig. 4. The scatterplot of the transparency inversion value and the measured value is evenly
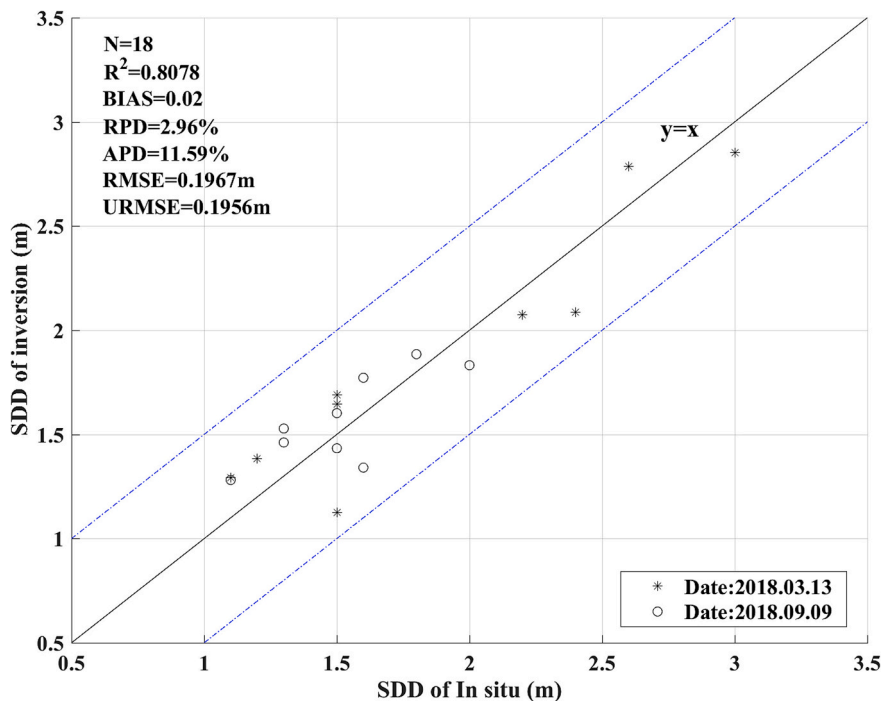
Fig. 4. Comparison of SDD estimated value and measured value

distributed on both sides of the 1:1 line. The determination coefficient of the algorithm model obtained from 18 groups of validation data is 0.8078, and the unbiased root mean square error is 0.1956 m, indicating that the model has high accuracy and can be used for inversion of water clarity in this area.

3.2. Temporal variation in SDD

As the sea water depth on the north and west sides of JZB is relatively shallow, it is greatly influenced by Dagu River, Yanghe River, Baisha River and other rivers. Besides, tide has a great influence on the water
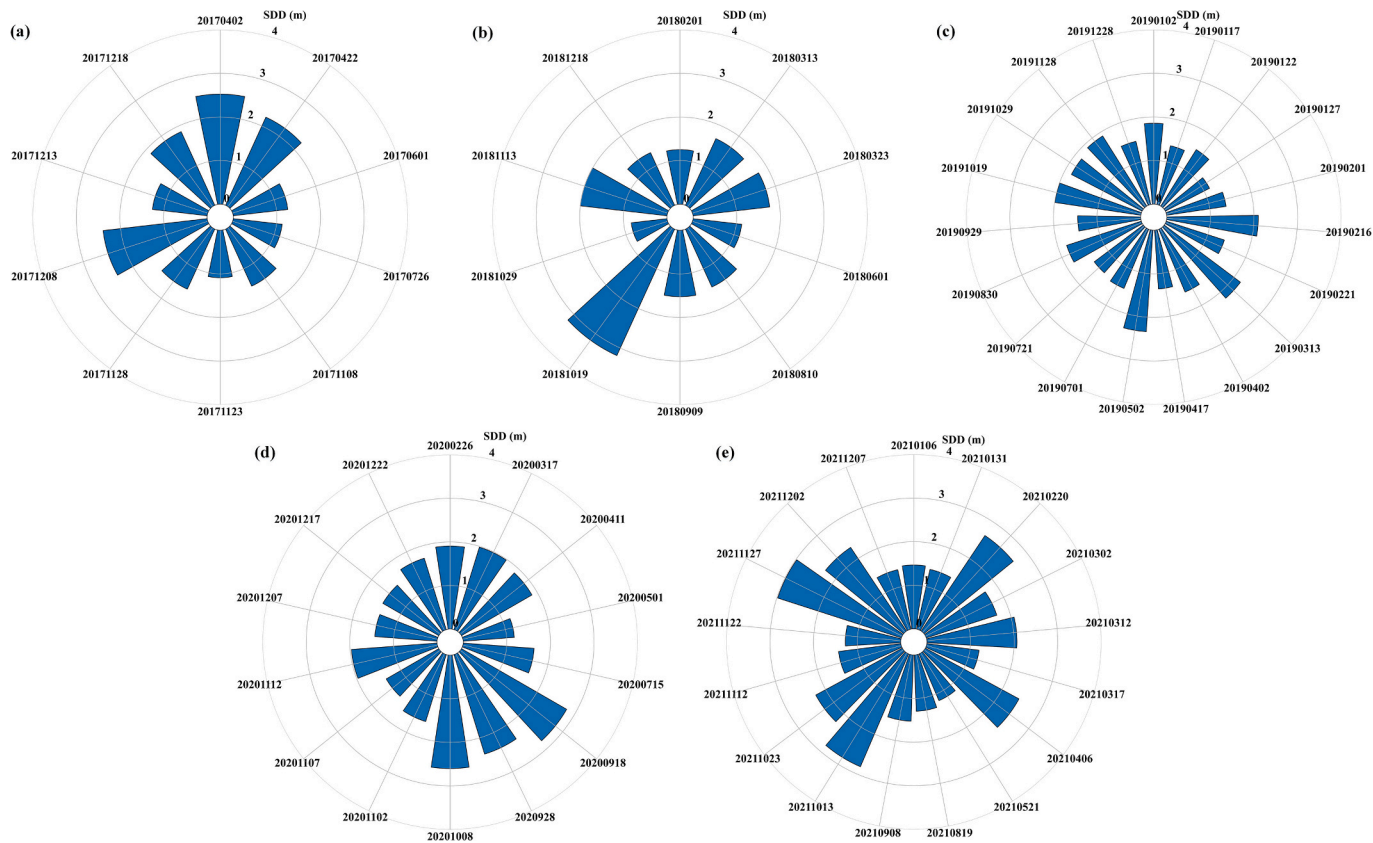
Fig. 5. The daily average SDD in JZB from 2017 to 2021 (a – e).

depth in this area. There is basically no sea water coverage in this area at low tide, so accurate and effective transparency inversion results cannot be obtained. Therefore, in this paper, the water clarity of inversion in this area is eliminated. The transparency inversion model of JZB constructed is used to carry out remote sensing inversion analysis of all valid Sentinel-2 MSI images of JZB from 2017 to 2021, and the water clarity distribution map of this area with 70 images is obtained. The mean distribution of transparency of the 70 images is shown in Fig. 5.

On this basis, all image results are ensemble averaged according by month, season and year, and the monthly and seasonal mean changes of water clarity in JZB are shown in Fig. 6, while the annual mean changes are shown in Fig. 7.

According to the analysis of the monthly mean and seasonal mean changes of transparency from 2017 to 2021, the mean SDD in JZB varies from 1.19 m to 2.07 m, with the monthly maximum value of 2.07 m in October and the minimum value of 1.19 m in June. With the change of seasons in spring, summer, autumn and winter, the mean SDD in JZB shows a trend of decrease, increase and decrease. The mean SDD is the smallest in summer (June, July and August) and the largest in autumn (September, October and November). The average value of transparency in spring (March, April and May) is slightly lower than that in autumn, and the value in winter (December, January and February) is slightly higher than that in summer.

According to the analysis results of SDD, during the five years from 2017 to 2021, the water clarity of JZB decreases from 2017 to 2018, and increases in the rest of the years. The overall water clarity of JZB shows an upward trend, among which, the smallest mean value of water clarity in 2018 is 1.61 m, while the largest mean value of water clarity in 2021 was 1.87 m, and the mean value of water clarity changed the most between 2019 and 2020, increasing by 0.15 m.

3.3. Spatial variation in SDD

Judging from the spatial distribution of the quarterly mean (Fig. 8) and annual mean of SDD (Fig. 9) in JZB during the five-year period from 2017 to 2021, the overall SDD in JZB shows characteristics of high in the south while low in the north, and high in the center while low in the surrounding areas. Most of the areas with SDD of >2 m are located in the southern waters of Jiaozhou Bay Bridge, and the areas with SDD of <2 m in the northern waters of JZB. The SDD shows more obvious texture features influenced by tides in the shallow water depth of the northwest region, whereas, the SDD presents local reduction occurring in the sea area near the mouth of JZB.

It can be seen from the spatial distribution of the seasonal mean of SDD in Fig. 8 that the overall SDD of <2 m in JZB is the lowest in summer, whereas, the overall SDD in the central sea area of JZB in winter is higher than that in summer. However, the SDD in most sea areas have remained low. Compared with summer and winter, the SDD in JZB has been significantly improved in spring and autumn. Besides, the overall SDD in the southern sea area of Jiaozhou Bay Bridge is higher than 2 m. Although the overall SDD in the northern part of Jiaozhou Bay Bridge is lower than 2 m, it has also increased compared with summer and winter.

As is seen from Fig. 9, the annual mean of the spatial distribution of SDD in JZB in 2018 is lower than that in 2017. During the five-year observation period, the annual mean of SDD in 2018 is the smallest as a whole, with the overall mean of the spatial distribution of SDD in JZB being <2 m. However, the annual mean SDD of >2 m merely happens in a small scope of JZB. The annual mean of the spatial distribution of SDD in the area in 2019 has slightly improved compared with that in 2018, and the annual mean of SDD in the central sea area of JZB has reached 2 m. In 2020 and 2021, the annual mean of the spatial distribution of SDD has greatly improved with the annual mean of SDD in the central sea area of JZB and the southern area of Jiaozhou Bay Bridge exceeding 2 m.

In addition to the mean distribution of SDD in the Bay area, there are many local real-time variations in SDD in JZB. As is shown in Fig.10(b, d & h), some strip-shaped SDD changes surge abruptly in the northwestern and northern waters of the Bay area. As is shown in Fig. 10(b, f, g & i), the SDD near the Bay mouth increases in a planar and linear manner. As is shown in Fig. 10(e), in the area with high overall SDD value in the northern part of the Bay mouth, the SDD abnormally decreases in the form of a curved line. As is shown in Fig. 10(a), the overall SDD in the Bay area changes indistinctively, and only a strip-shaped area in the northwest sea area presents a significant decrease.

4. Discussion

Similar to other nearshore semi-enclosed bays, the ecological environment in JZB is mainly affected by both natural and human factors which exert obvious influence on variation in SDD. The natural factors affecting variation in SDD in JZB mainly include the components of the water body (mainly including chlorophyll, suspended solids and colored soluble organic matter), rainfall, river runoff, wind velocity, temperature, water depth, tide, current, water mass and geographical location. Human factors mainly include coastline changes, aquaculture, bridge facility construction, sewage discharge, port construction, and ship navigation. The main factors influencing the change of SDD in JZB are shown in Fig. 11.
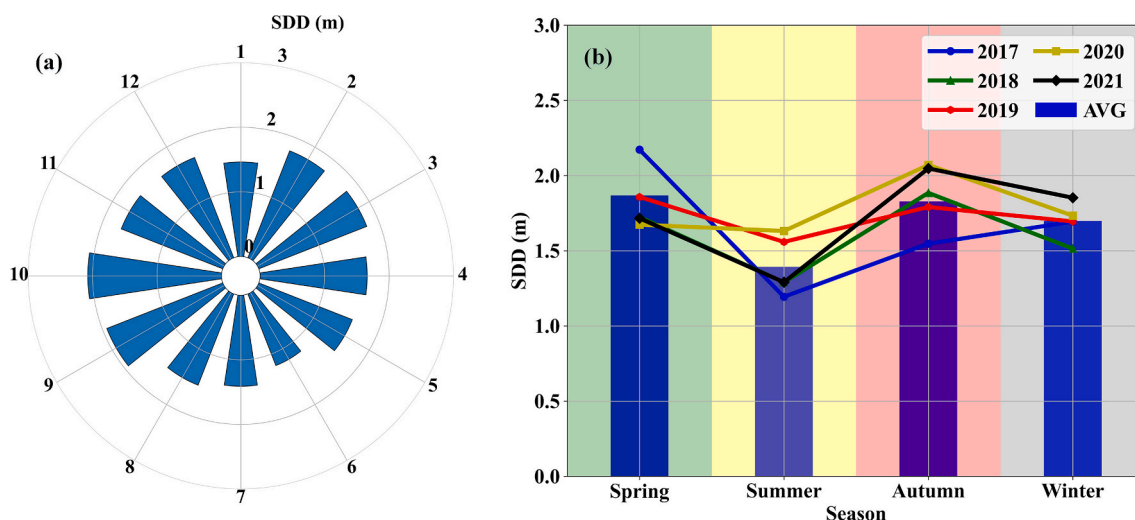

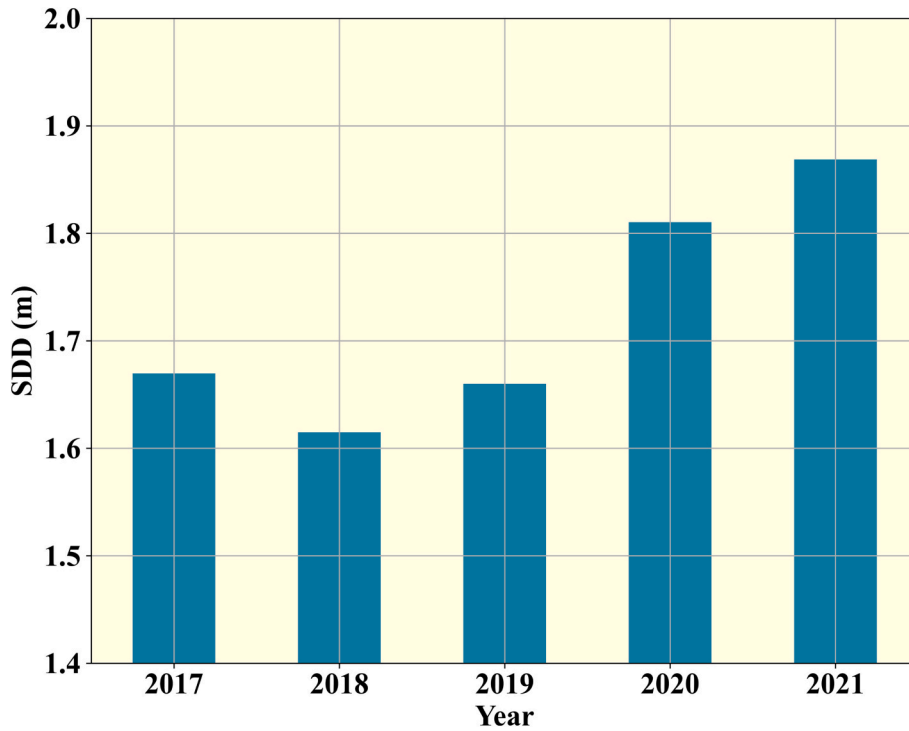**Fig. 6.** Monthly (a) and quarterly (b) mean SDD in JZB from 2017 to 2021.

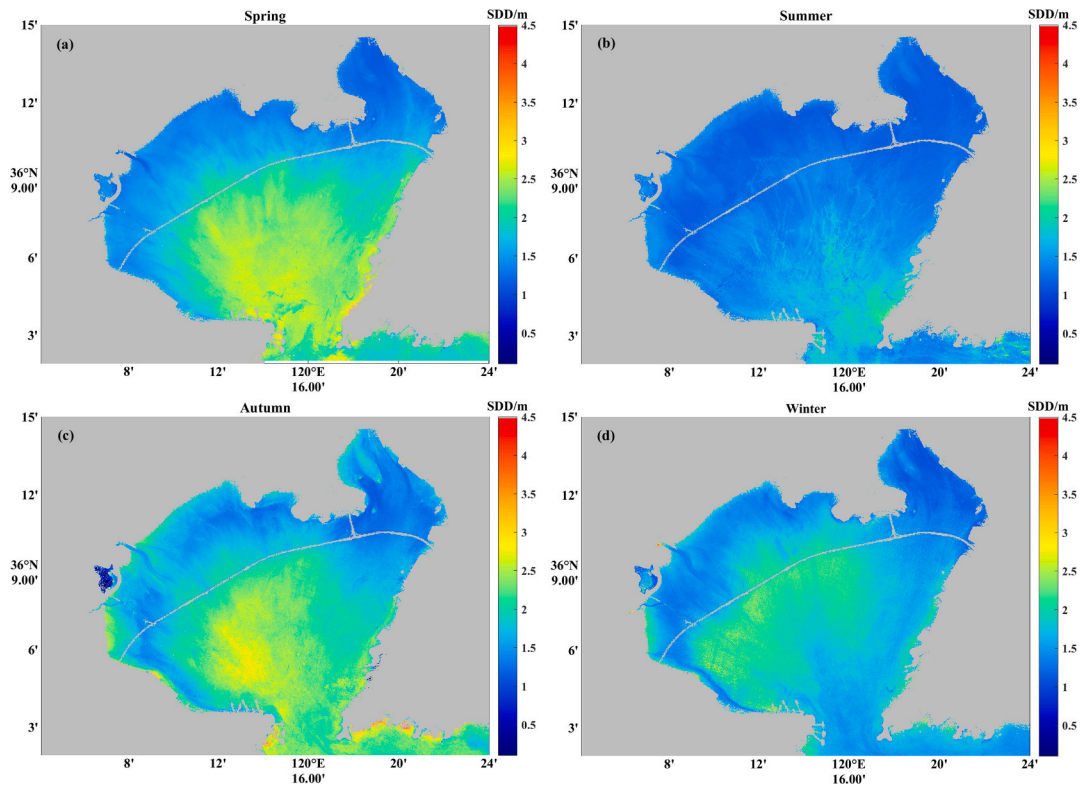**Fig. 7.** Annual mean SDD in JZB from 2017 to 2021.

Fig. 8. Spatial distributions of seasonal mean SDD in JZB from 2017 to 2021 (a-d).

4.1. Natural factors

Natural factors such as rainfall, wind velocity, and temperature all exert direct or indirect effects on SDD. In this paper, relevant analyses were made by adopting the measured rainfall, wind speed and temperature data ranging from 2017 to 2021, derived from the National Field Scientific Observation and Research Station of Jiaozhou Bay Marine Ecosystem in Shandong Province. The runoff of rivers will bring a large amount of suspended sediment into the sea area, which proves another important factor affecting SDD of the area. The inflow rivers in
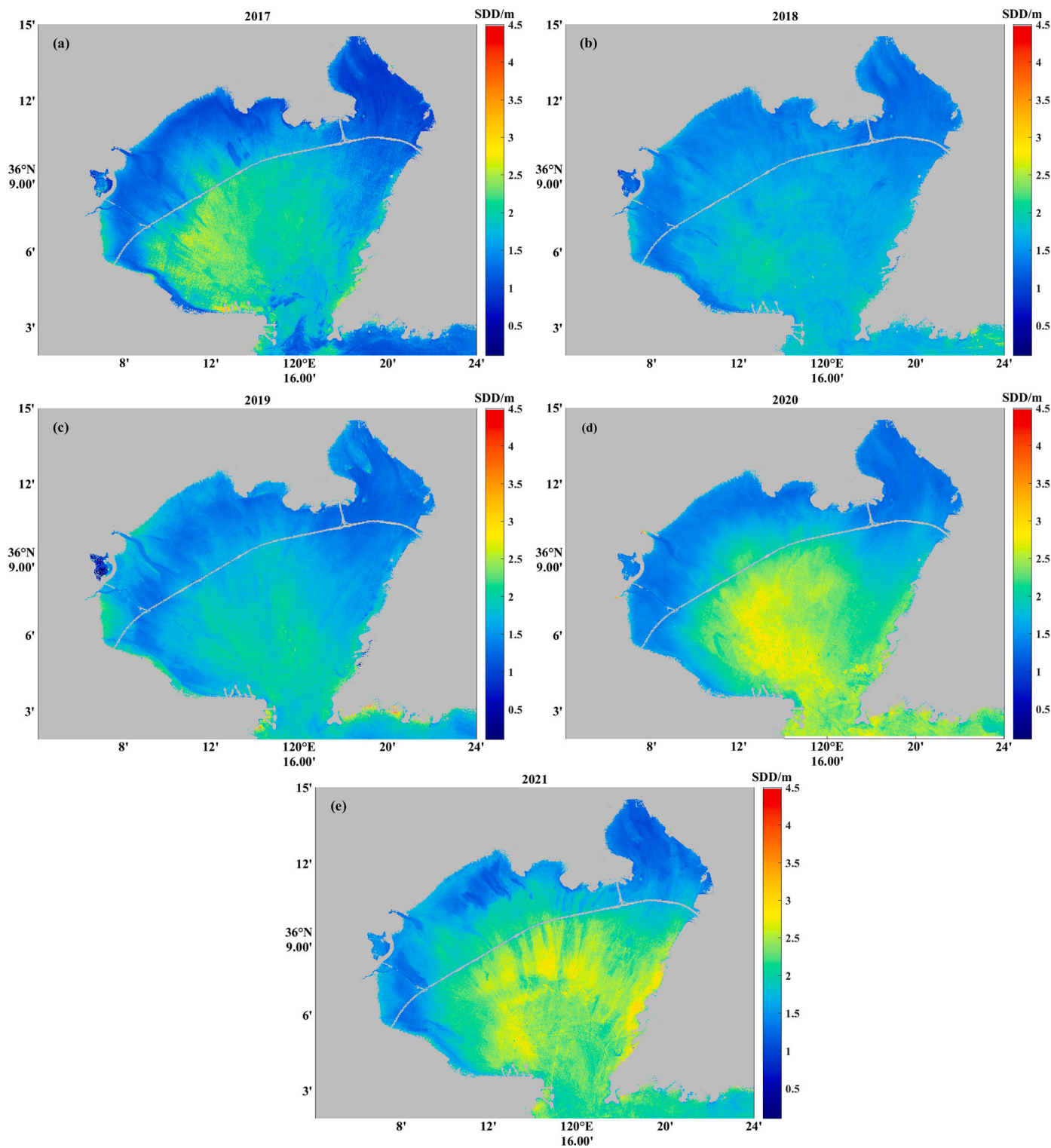
Fig. 9. Spatial distributions of annual mean SDD in JZB from 2017 to 2021 (a-e).

JZB (including Dagu River, Baisha River, Yanghe river and Licun River, etc.) are rain-source rivers, therefore, the variation of rainfall directly reflects the runoff of the inflow rivers into JZB.

The SDD in JZB from 2017 to 2021 were averaged by month, so were the obtained data of rainfall, wind velocity and air temperature, and a comparative analysis of these data was conducted over 12 months. As is seen from Fig. 12, the SDD in JZB is basically negatively correlated with rainfall and temperature. The average rainfall and temperature in

summer (June, July and August) reach upon the highest stage. The abundant rainfall will increase the runoff of all rain-source rivers (including Dagu River, Baisha River, Yanghe River, Licun River, etc.) inflowing into the sea area, which will increase the sediment content in the area, finally resulting in the surge of suspended matter content in the waters and deduction of SDD. Meanwhile, the increase of temperature in June, July and August makes more fertile grounds for phytoplankton growth in the water, which will greatly increase the content of
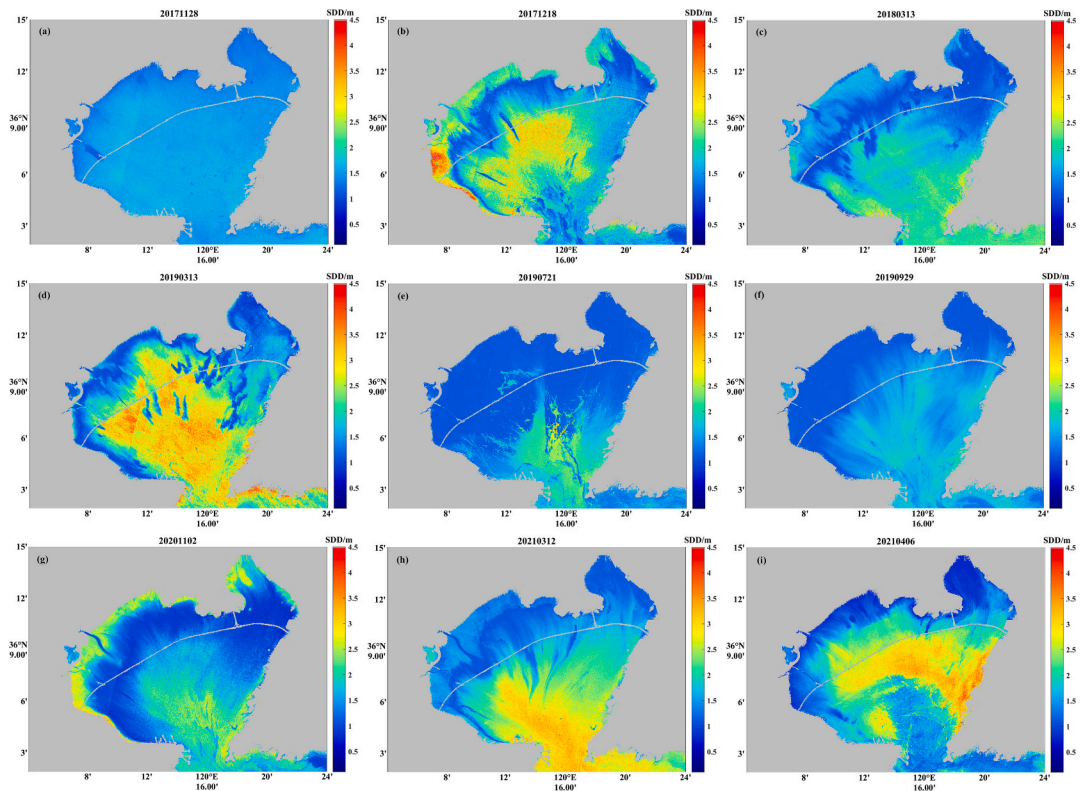
Fig. 10. Spatial distributions of daily mean SDD in JZB from 2017 to 2021 (a-i).
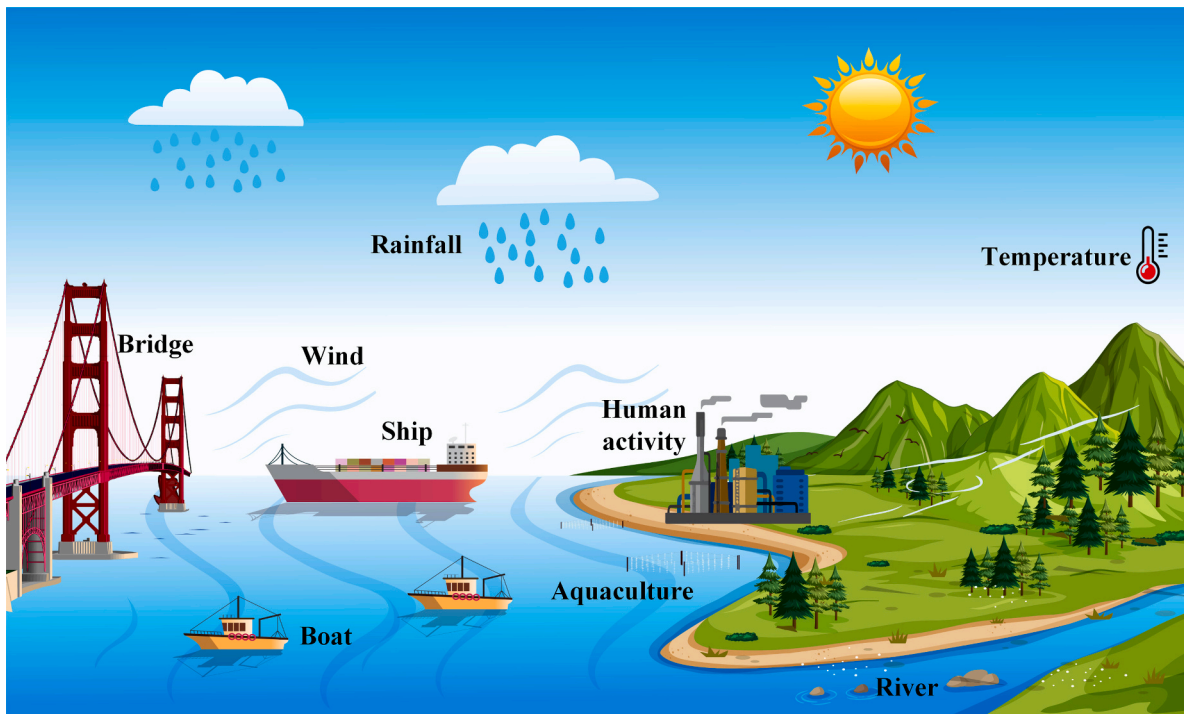

Fig. 11. Natural and human factors affecting water clarity

chlorophyll in the water, reducing SDD significantly. Except for June, July and August in summer, the less monthly average rainfall (<50 mm) and lower temperature (below 20 °C) in JZB have little influence on SDD. Among all the natural factors, wind velocity plays a more important role in SDD, particularly in the northwest, north and northeast

waters where the sea depth is shallow. As is shown in Fig. 12, the stronger wind velocity will bring more suspended sediment in the water (especially for shallow water) to lower SDD, and thus, variation in SDD in other months except June, July and August shows a significant negative correlation with wind velocity.
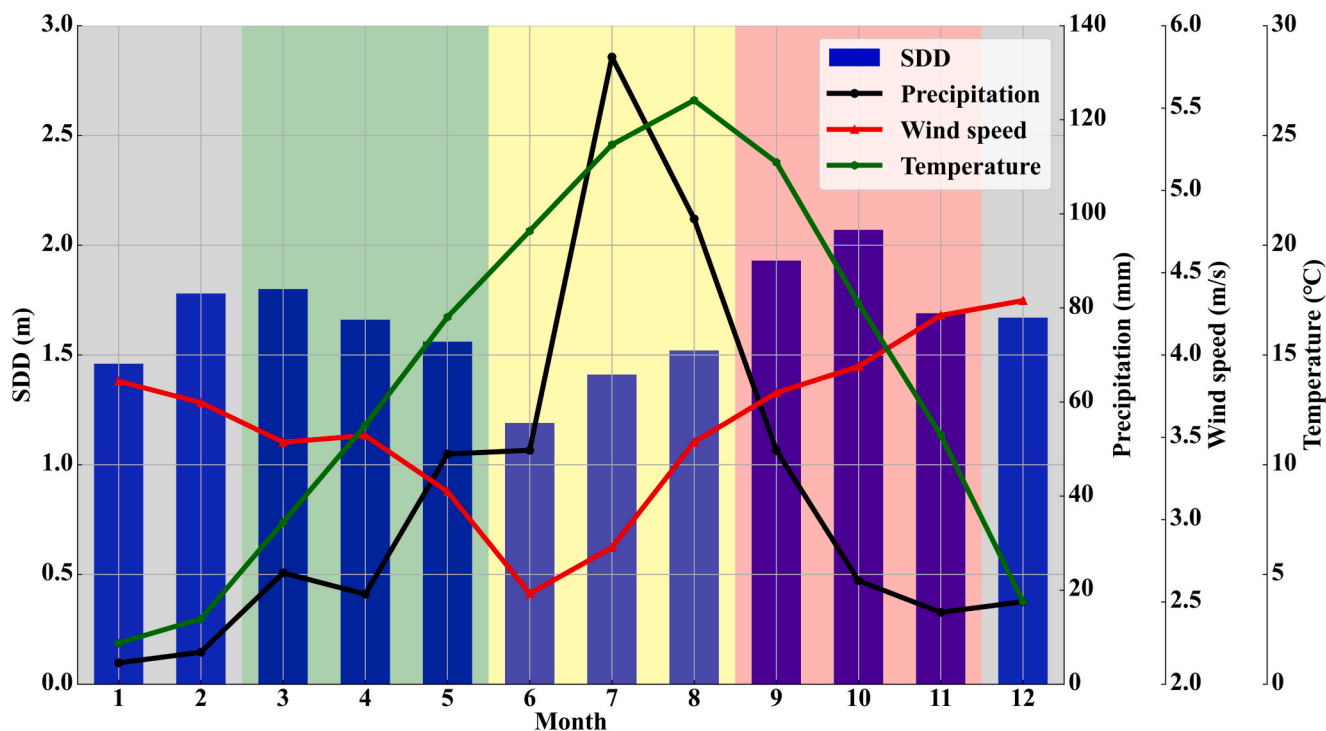
Fig. 12. The relationship between the monthly mean SDD and the monthly mean rainfall, wind speed and temperature in JZB from 2017 to 2021.

The correlation coefficient and significance test results of SDD with precipitation, temperature and wind speed are shown in Table 2. Considering that precipitation and temperature in June, July and August play a dominant role in SDD, wind speed has little impact. Therefore, the results of June, July and August are removed when calculating the correlation and significance of SDD and wind speed. Table 2 shows that SDD is negatively correlated with precipitation, temperature and wind speed, which is consistent with the results obtained in the previous analysis. The *p* values of the significance test results are all <0.01, indicating that the negative correlation results are extremely significant.

The annual average comparison and analysis were conducted for SDD on JZB from 2017 to 2021, as well as the obtained data of rainfall, wind velocity, and temperature, as is shown in Fig. 13. It can be seen that because of unobvious variation in the annual mean value of wind velocity and temperature, wind velocity and temperature cannot dominate the annual variation in SDD. The annual rainfall is the smallest in 2019, and there is little difference in rainfall in other years, with the difference in annual rainfall of <150 mm. Meanwhile, without correlation between changes in the annual mean of SDD and annual rainfall, annual rainfall cannot play a dominant role in variation in the annual mean of SDD.

In addition to the above natural factors such as rainfall, wind speed and temperature, there are also some short-term natural factors that can affect SDD in JZB. For example, *Enteromorpha prolifera* often breaks out in the Yellow Sea in July and August every year. JZB is connected with the Yellow Sea, and it is also affected by *enteromorpha prolifera*. As shown in Fig. 10(e), in the sea area around the mouth of JZB, there are some long and narrow changes showing linear and areal abnormal decrease in SDD. Compared with the satellite image synthesized in the red, green and blue bands in Fig. 14, it can be seen that this abnormal

decrease in SDD is caused by the outbreak of *enteromorpha prolifera*.

4.2. Human factors

In addition to natural factors, variation in SDD mainly stems in part from human factors. Recent years have witnessed the spurt of progress in society and economy and the implementation of relevant ecological protection policies in JZB, affecting variation in SDD of the area. Among all the human factors, human activities have a major influence on the nearshore water body and the water body in the bay, chiefly triggering variation in SDD.

4.2.1. Coastline changes

The change of coastline types in JZB is an important indicator reflecting human activities along the coast of JZB. The change data of coastline types in JZB in this paper were derived from the length data of various types of coastlines in China's coastline from 2017 to 2021 according to the statistics of the Ministry of Ecology and Environment. The overall analysis and comparison of the coastline types in the whole JZB were carried out, with the results shown in Fig. 15.

It can be seen that the proportion of natural coastlines and artificial coastlines in JZB has changed little in the past five years with the slight decrease in the proportion of natural coastlines and the subtle increase in that of artificial coastlines. However, natural coastlines have little impact on the environment. Artificial coastlines, reflecting the changes of various human activities in the region, exert a major impact on the water body. The changes in the proportion of various coastlines in artificial coastlines are shown in Fig. 16.

Artificial coastlines mainly include aquaculture coastlines, embankment construction, wharf coastlines and traffic embankments. The four types of artificial coastlines have diverse impacts on the water body, among which the aquaculture coastlines have the greatest impact while the traffic embankments have the least impact. By comparing the charts of annual average variation in SDD (Fig. 7), it can be seen that the SDD in JZB decreases from 2017 to 2018, and increases from 2018 to 2021, which is also consistent with the changes in the proportion of aquaculture coastlines. Moreover, compared with the impact of
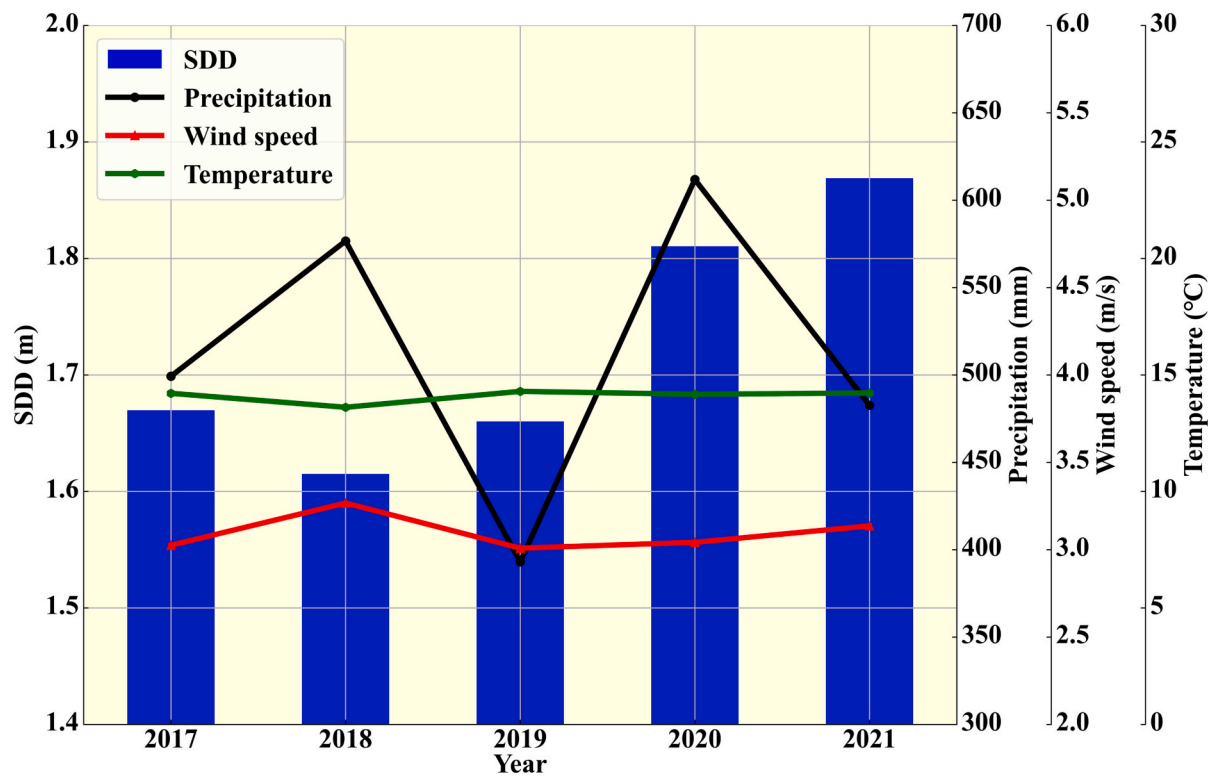
Table 2
Correlation coefficient and significance test results of SDD and its influencing factors.

		Precipitation	Temperature	Wind speed
SDD	r	−0.53	−0.34	−0.22
	p	2.67×10^{-3}	2.47×10^{-4}	1.31×10^{-5}

Fig. 13. The relationship between the annual mean SDD and the annual mean rainfall, wind speed and temperature in JZB from 2017 to 2021.

aquaculture coastlines on the transparency of water body, the other three artificial coastlines, i.e. embankment construction, wharf coastlines and traffic embankments, influence SDD less obviously.

4.2.2. Port and navigation

The change of coastlines mainly affects the nearshore SDD in the sea area. Because ship navigation will leave suspended solids such as sediment in the water body lifted, and cause pollution discharge and oil spill (Dong et al., 2022), variation in SDD in the central waters of the Bay area is thus affected. With the large Qingdao Port located in JZB, the throughput of the port can directly reflect the navigation frequency of ships in the area. According to the annual report of Qingdao Port in recent five years, the cargo and container throughput of the port from 2017 to 2021 is shown in Fig. 17.

It can be seen that from 2017 to 2021, the cargo and container throughput of the entire Qingdao Port has been edging upwards year by year, and the annual throughput basically shows a linear increase, of which the increase slightly slowed down from 2019 to 2020. However, the annual mean variation in SDD only decreases from 2017 to 2018, and the rest of the years saw an increase in SDD. This trend is not entirely consistent with the reduction of SDD caused by ship navigation, mainly because this kind of reduction happens in just a short period of time. As is shown in Fig. 10 (c, f, g), the SDD caused by the ship navigation is reduced in the shape of slim and short lines near the mouth of the bay and the waters near the northern part of the bay. As is shown in Fig. 10 (c, d) in the sea area near Jiaozhou Bay Bridge, the SDD caused by the oil leakage of fishing boats shows a local planar decrease. It is observed on the spot that the oil spill pollution in JZB mostly occurs on the northeast and northwest side of the sea area near Jiaozhou Bay Bridge. As is shown in Fig. 18, this is caused by rows of small fishing boats navigating and berthing off. The above situations will give rise to short-term decrease in SDD, but with unobvious influence on the annual average SDD. Meanwhile, reduction in SDD caused by ship navigation only occurs in the channel area, with little effect on the entire JZB.

4.2.3. Jiaozhou Bay Bridge

Founded on December 26, 2006, Jiaozhou Bay Bridge started construction in May 2007 and completed in June 2011. During the observation period of remote sensing images from 2017 to 2021 in this paper, the bridge has been completed and operated for many years, with only the Jiaozhou connecting line section of Jiaozhou Bay Bridge under construction. Started on March 7, 2017, the Jiaozhou connecting line section of Jiaozhou Bay Bridge was completed on December 28, 2019.

According to the seasonal, annual and diurnal spatial distribution variation of SDD in JZB in Figs. 8, 9 and 10, the influence of the construction of the bridge on SDD in the Bay area cannot be observed. This is mainly due to the fact that JZB is a highly enclosed bay (the sea area covers an area of nearly 400 km², and the inlet to the bay is only approximately 3 km wide); meanwhile, because the rivers emptying into the bay are mostly rain-source rivers, the overall runoff stays at a low level, leaving the hydrodynamic force in the bay not as violent as that in Hangzhou Bay and the Guangdong-Hong Kong-Macao Greater Bay Area. Therefore, although Jiaozhou Bay Bridge has some unobvious impact on the hydrodynamics in the Bay area, the SDD variation caused by the bridge is not significant.

Located in the northwest of JZB, the sea area of the Jiaozhou connecting line section of Jiaozhou Bay Bridge is shallow, with basically no sea water coverage especially at low tidal levels. When analyzing the spatial distribution of SDD in this area, it is necessary to select remote sensing images that are imaged at high tidal levels. In Fig. 10 (a), due to the imaging time during the period of high tidal levels, the SDD in the Bay area shows well-proportioned spatial distribution as a whole, but abnormally reduces only in the sea area of Jiaozhou connecting line section of Jiaozhou Bay Bridge. However, on November 28, 2017, this section of Jiaozhou Bay Bridge was under construction, obviously causing the spatial variation in the reduction of SDD in the construction area.

4.2.4. COVID-19

In December 2019, the COVID-19 pandemic broke out in Wuhan City

Fig. 14. Satellite image of JZB synthesized by the red, green and blue bands on July 21, 2019 (For interpretation of the references to color in this figure legend, the reader is referred to the web version of this article.)

of China. On January 17, 2020, the first case was confirmed in Qingdao City. Thanks to the adoption of pandemic control policies by Qingdao City, many companies were closed or operated from home. Therefore, human activities along the coast of JZB and in the bay were also plummeted, which had a direct impact on the ecological environment of JZB, such as directly reducing the amount of industrial wastewater discharged into the Bay area and affecting fishing and aquaculture as well as engineering construction along the coast to a certain extent. The reduction and weakening of these human activities will improve the ecological environment in the sea area greatly. It can be seen from Fig. 7, the SDD of JZB has increased from 2018 to 2021, particularly from 2019 to 2020 at the highest rate, which also reflects the impact of reduced human activities on variation in SDD in JZB.

5. Conclusions

In this paper, Sentinel-2 MSI imagery and the established SDD inversion model of JZB were used to obtain SDD inversion data of JZB from 2017 to 2021. Subsequently, the temporal and spatial distribution of SDD in JZB in the past five years was analyzed, together with the main characteristics of SDD variation and the main factors. The conclusions are as follows:

(1) Temporal variation distribution law of SDD in JZB: From 2017 to 2021, the annual average SDD variation in JZB, on a downward trajectory initially, has risen subsequently. In 2018, the average annual SDD is 1.61 m, reaching the lowest level. In 2021, the annual average SDD is 1.87 m, reaching the highest stage. From
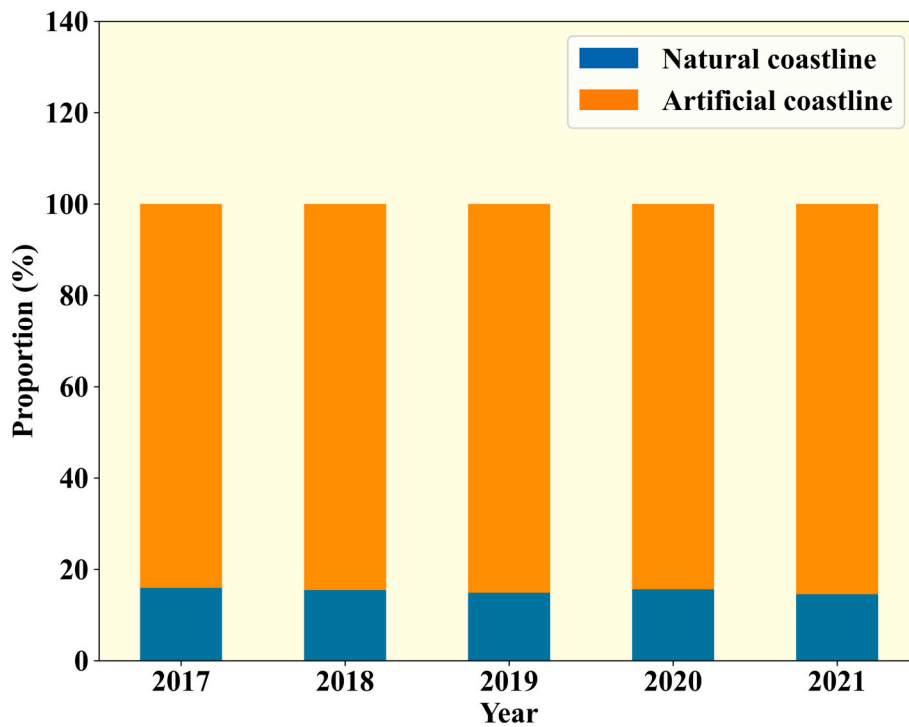
Fig. 15. Changes in the proportion of natural coastlines and artificial coastlines in JZB from 2017 to 2021.
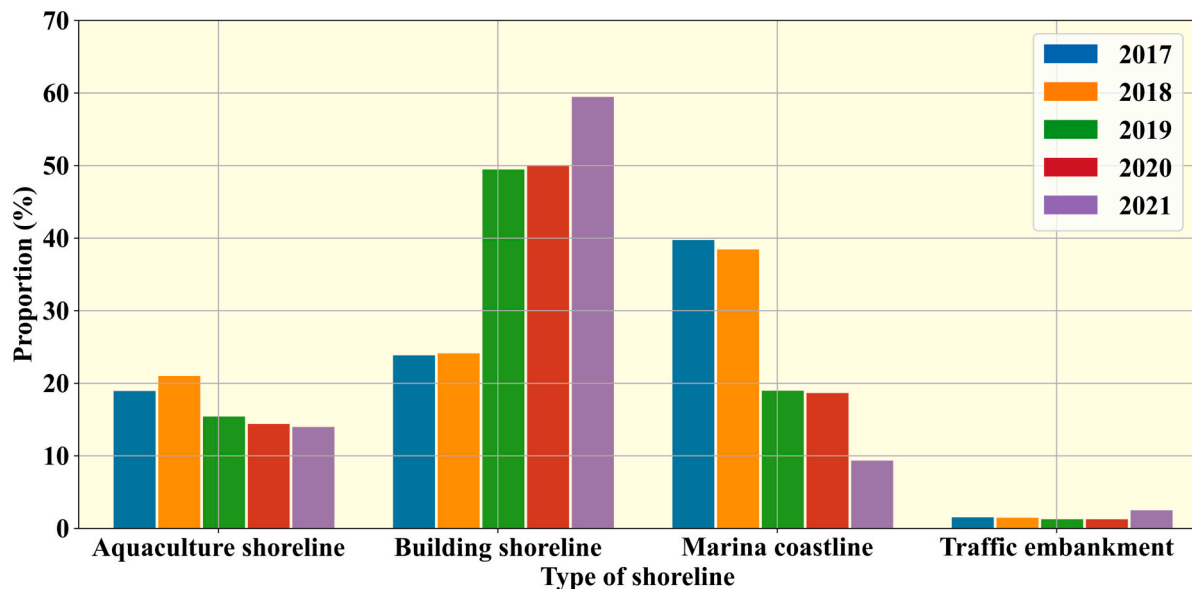

Fig. 16. Changes in the proportion of various artificial coastlines in JZB from 2017 to 2021.

2019 to 2021, the annual average SDD changes the most, increasing by 0.15 m. With the rhythm of the seasons, the seasonal average SDD of JZB goes through a trend of decreasing, increasing and then decreasing, in which the average SDD in summer is the lowest, followed by winter, and the highest in spring and autumn.

(2) Spatial variation distribution law of SDD in JZB: The spatial distribution of the average SDD has the features of low in the north, high in the south, high in the center, and low in the surrounding areas. The distribution of SDD in the shallower waters in the west and north forms the texture characteristics influenced by tides. In the bay mouth and the waters to the north of the bay mouth, SDD shows the short-term decrease in a linear variation form caused by ship navigation. The SDD distribution in the northern and eastern sea areas has decreased in variation forms of strip and plane caused by oil leakage. In July and August, there will be the distribution variation of SDD decreasing caused by *enteromorpha prolifera*.

(3) Natural factors such as rainfall, wind velocity, and temperature will affect the variation in SDD of JZB. Among them, the increasing rainfall will increase the runoff of the rivers flowing into the Bay area, which in turn will bring more content of suspended solids such as sediment into the area, resulting in a decrease in SDD. Therefore, rainfall is considered as the main
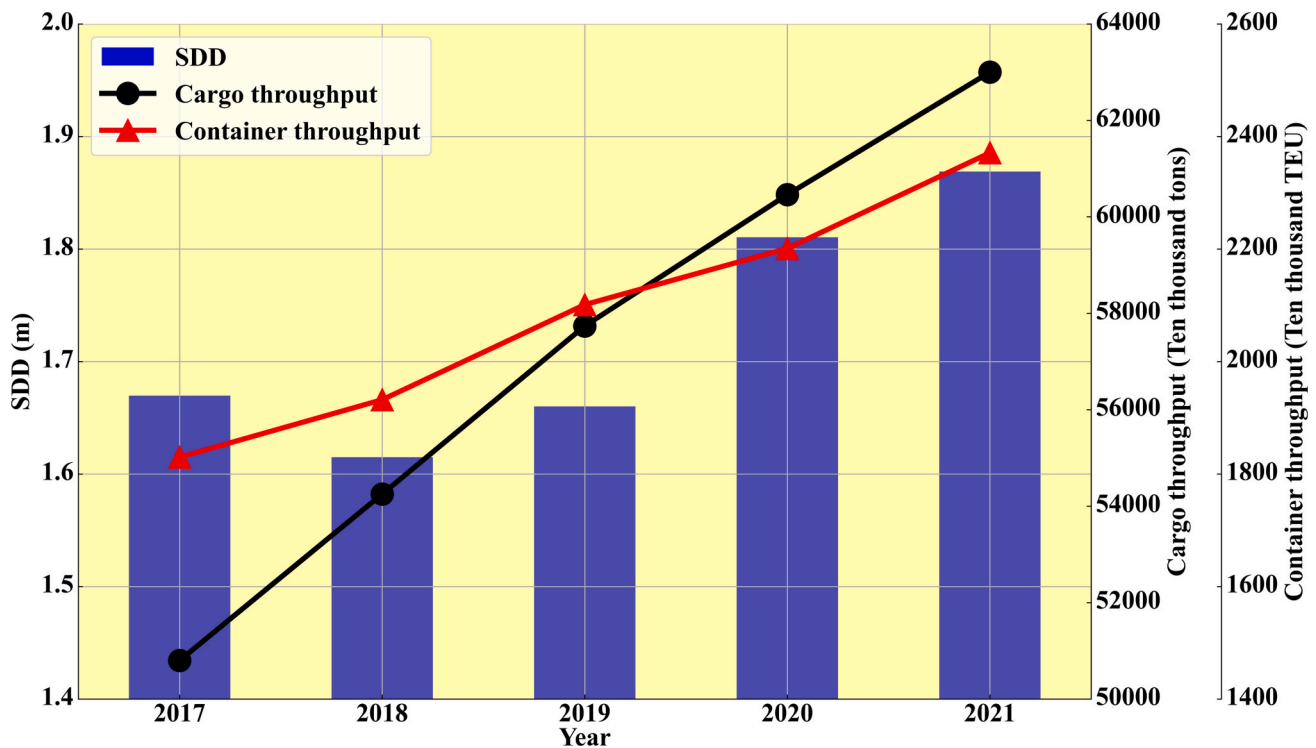
Fig. 17. SDD and throughput changes of Qingdao Port in JZB from 2017 to 2021.
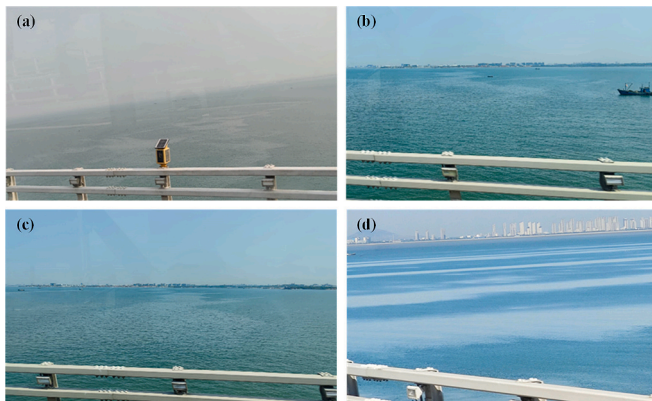

Fig. 18. Oil spill scene in the northern waters of JZB

factor affecting variation in SDD of JZB. Besides, for the shallow water area, the stronger wind velocity will cause sediment suspension in the bottom of the water, leading to reduction of SDD. Thus, wind velocity proves to be the dominant factor affecting variation in SDD on the premise of less rainfall. Finally, temperature will affect the growth and reproduction of chlorophyll in JZB, further influencing variation in SDD. Natural factors play a dominant role in the monthly and quarterly distribution variation of SDD, but not in the annual distribution variation.

(4) Human activities such as aquaculture, coastline type changes, port construction and development, ship navigation, and bridge construction are taken as the primary human-induced factors that cause variation in SDD in JZB. As the main human-induced factor among these human activities, aquaculture has the greatest impact on variation in SDD. Ship navigation and the construction of Jiaozhou Bay Bridge will cause the distribution variation of short-term decrease in SDD in a small area. At the beginning of 2020, human activities slip considerably due to the outbreak of

COVID-19 pandemic, triggering the maximum increase of SDD from 2019 to 2020, which reflects the great impact of human activities on variation in SDD of JZB. Human factors play a leading role in the annual distribution variation in SDD rather than in the monthly and seasonal distribution variation.

CRediT authorship contribution statement

Lei Yang: Conceptualization, Data curation, Formal analysis, Methodology, Visualization, Writing – review & editing. **Dingfeng Yu:** Conceptualization, Methodology, Funding acquisition, Writing – review & editing. **Huiping Yao:** Data curation, Software. **Hao Gao:** Investigation, Formal analysis. **Yan Zhou:** Formal analysis. **Yingying Gai:** Visualization, Resources. **Xiaoyan Liu:** Resources. **Maosheng Zhou:** Investigation. **Shunqi Pan:** Writing – review & editing.

Declaration of competing interest

The authors declare that they have no known competing financial interests or personal relationships that could have appeared to influence the work reported in this paper.

Data availability

The authors do not have permission to share data.

Acknowledgments

References

An, D., Xing, Q., Yu, D., Pan, S., 2022. A simple method for estimating macroalgae area under clouds on MODIS imagery. Front. Mar. Sci. 9 https://doi.org/10.3389/fmars.2022.995731.

Cai, H., Li, C., Luan, X., Ai, B., Yan, L., Wen, Z., 2022. Analysis of the spatiotemporal evolution of the coastline of Jiaozhou Bay and its driving factors. Ocean & Coastal Management 226, 106246. https://doi.org/10.1016/j.ocecoaman.2022.106246.

Chusnah, W.N., Chu, H.-J., 2022. Estimating chlorophyll-a concentrations in tropical reservoirs from band-ratio machine learning models. Remote Sensing Applications: Society and Environment 25, 100678. https://doi.org/10.1016/j.rsase.2021.100678.

Dong, Y., Liu, Y., Hu, C., MacDonald, I.R., Lu, Y., 2022. Chronic oiling in global oceans. Science 376 (6599), 1300–1304. https://doi.org/10.1126/science.abm5940.

Doron, M., Babin, M., Hembise, O., Mangin, A., Garnesson, P., 2011. Ocean transparency from space: validation of algorithms estimating secchi depth using MERIS, MODIS and SeaWiFS data. Remote Sens. Environ. 115 (12), 2986–3001. https://doi.org/10.1016/j.rse.2011.05.019.

He, X., Pan, D., Bai, Y., Wang, T., Chen, C.-T.A., Zhu, Q., Hao, Z., Gong, F., 2017. Recent changes of global ocean transparency observed by SeaWiFS. Cont. Shelf Res. 143, 159–166. https://doi.org/10.1016/j.csr.2016.09.011.

He, Y., Lu, Z., Wang, W., Zhang, D., Zhang, Y., Qin, B., Shi, K., Yang, X., 2022. Water clarity mapping of global lakes using a novel hybrid deep-learning-based recurrent model with landsat OLI images. Water Res. 215, 118241 https://doi.org/10.1016/j.watres.2022.118241.

Kabiri, K., 2022. Estimation of the secchi disk depth from the NASA MODIS-aqua diffuse attenuation coefficient data in the northern persian gulf and the Gulf of Oman: a spatiotemporal assessment. Reg. Stud. Mar. Sci. 52, 102359 https://doi.org/10.1016/j.rsma.2022.102359.

Kloiber, S.M., Brezonik, P.L., Olmanson, L.G., Bauer, M.E., 2002. A procedure for regional lake water clarity assessment using landsat multispectral data. Remote Sens. Environ. 82 (1), 38–47. https://doi.org/10.1016/S0034-4257(02)00022-6.

Lee, Z., Shang, S., Hu, C., Du, K., Weidemann, A., Hou, W., Lin, J., Lin, G., 2015. Secchi disk depth: a new theory and mechanistic model for underwater visibility. Remote Sens. Environ. 169, 139–149. https://doi.org/10.1016/j.rse.2015.08.002.

Li, L., Xing, Q., Li, X., Yu, D., Zhang, J., Zou, J., 2018. Assessment of the impacts from the World's largest floating macroalgae blooms on the water clarity at the West Yellow Sea using MODIS data (2002–2016). IEEE Journal of Selected Topics in Applied Earth Observations and Remote Sensing 11 (5), 1397–1402. https://doi.org/10.1109/jstars.2018.2806626.

Liu, D., Duan, H., Loiselle, S., Hu, C., Zhang, G., Li, J., Yang, H., Thompson, J.R., Cao, Z., Shen, M., Ma, R., Zhang, M., Han, W., 2020. Observations of water transparency in China's lakes from space. Int. J. Appl. Earth Obs. Geoinf. 92, 102187 https://doi.org/10.1016/j.jag.2020.102187.

Liu, C., Zhu, L., Li, J., Wang, J., Ju, J., Qiao, B., Ma, Q., Wang, S., 2021. The increasing water clarity of tibetan lakes over last 20 years according to MODIS data. Remote Sens. Environ. 253, 112199 https://doi.org/10.1016/j.rse.2020.112199.

Luo, J., Pu, R., Duan, H., Ma, R., Mao, Z., Zeng, Y., Huang, L., Xiao, Q., 2020. Evaluating the influences of harvesting activity and eutrophication on loss of aquatic vegetations in taihu Lake, China. Int. J. Appl. Earth Obs. Geoinf. 87, 102038 https://doi.org/10.1016/j.jag.2019.102038.

Maciel, D.A., Barbosa, C.C.F., Flores Júnior, R., Novo, E.M.L.D.M., Begliomini, F.N., 2021. Water clarity in Brazilian water assessed using Sentinel-2 and machine learning methods. ISPRS Journal of Photogrammetry and Remote Sensing 182, 134–152. https://doi.org/10.1016/j.isprsjprs.2021.10.009.

Main-Knorn, M., Pflug, B., Debaecker, V., Louis, J., 2015. Calibration and validation plan for the L2a processor and products of the Sentinel-2 Mission. Int. Arch. Photogramm. Remote. Sens. Spat. Inf. Sci. 40 (W3), 1249–1255. https://doi.org/10.5194/isprsarchives-XL-7-W3-1249-2015.

Majozi, N.P., Salama, M.S., Bernard, S., Harper, D.M., Habte, M.G., 2014. Remote sensing of euphotic depth in shallow tropical inland waters of Lake Naivasha using MERIS data. Remote Sens. Environ. 148, 178–189. https://doi.org/10.1016/j.rse.2014.03.025.

Mao, Y., Wang, S., Qiu, Z., Sun, D., Bilal, M., 2018. Variations of transparency derived from GOCI in the Bohai Sea and the Yellow Sea. Opt. Express 26 (9), 12191–12209. https://doi.org/10.1364/oe.26.012191.

Olmanson, L.G., Bauer, M.E., Brezonik, P.L., 2008. A 20-year landsat water clarity census of Minnesota's 10,000 lakes. Remote Sens. Environ. 112 (11), 4086–4097. https://doi.org/10.1016/j.rse.2007.12.013.

Pitarch, J., 2020. A review of Secchi's contribution to marine optics and the foundation of secchi disk science. Oceanography 33 (3), 26–37. https://doi.org/10.5670/oceanog.2020.301.

Qing, S., Cui, T., Lai, Q., Bao, Y., Diao, R., Yue, Y., Hao, Y., 2021. Improving remote sensing retrieval of water clarity in complex coastal and inland waters with modified absorption estimation and optical water classification using Sentinel-2 MSI. Int. J. Appl. Earth Obs. Geoinf. 102, 102377 https://doi.org/10.1016/j.jag.2021.102377.

Rohan, S.K., Kotwicki, S., Kearney, K.A., Schulien, J.A., Laman, E.A., Cokelet, E.D., Beauchamp, D.A., Britt, L.L., Aydin, K.Y., Zador, S.G., 2021. Using bottom trawls to monitor subsurface water clarity in marine ecosystems. Prog. Oceanogr. 194, 102554 https://doi.org/10.1016/j.pocean.2021.102554.

Sent, G., Biguino, B., Favareto, L., Cruz, J., Sá, C., Dogliotti, A.I., Palma, C., Brotas, V., Brito, A.C., 2021. Deriving water quality parameters using Sentinel-2 imagery: a case study in the Sado estuary. Portugal. Remote Sensing 13 (5), 1043. https://doi.org/10.3390/rs13051043.

Shan, J., Li, J., 2020. Valuing marine ecosystem service damage caused by land reclamation: insights from a deliberative choice experiment in Jiaozhou Bay. Mar. Policy 122, 104249. https://doi.org/10.1016/j.marpol.2020.104249.

Shang, S., Lee, Z., Wei, G., 2011. Characterization of MODIS-derived euphotic zone depth: results for the China Sea. Remote Sens. Environ. 115 (1), 180–186. https://doi.org/10.1016/j.rse.2010.08.016.

Shang, S., Lee, Z., Shi, L., Lin, G., Wei, G., Li, X., 2016. Changes in water clarity of the Bohai Sea: observations from MODIS. Remote Sens. Environ. 186, 22–31. https://doi.org/10.1016/j.rse.2016.08.020.

Sivakumar, R., Prasanth, B.R.S.V., Ramaraj, M., 2022. An empirical approach for deriving specific inland water quality parameters from high spatio-spectral resolution image. Wetl. Ecol. Manag. 30 (2), 405–422. https://doi.org/10.1007/s11273-022-09874-4.

Song, K., Wang, Q., Liu, G., Jacinthe, P.-A., Li, S., Tao, H., Du, Y., Wen, Z., Wang, X., Guo, W., Wang, Z., Shi, K., Du, J., Shang, Y., Lyu, L., Hou, J., Zhang, B., Cheng, S., Lyu, Y., Fei, L., 2022. A unified model for high resolution mapping of global lake (>1 ha) clarity using landsat imagery data. Sci. Total Environ. 810, 151188 https://doi.org/10.1016/j.scitotenv.2021.151188.

Su, W., Zhang, M., Jiang, K., Zhu, D., Huang, J., Wang, P., 2018. Atmospheric correction method of Sentinel-2 satellite imagery. Acta Opt. Sin. 38 (1), 322–331.

Tyler, J.E., 1968. The secchi disc. Limnol. Oceanogr. 13 (1), 1–6.

Wang, N., Li, J.-M., Xu, Z.-H., 2021. Public preference for the ecological restoration of coastal wetlands in Jiaozhou Bay in China based on a choice experiment. Mar. Policy 128, 104487. https://doi.org/10.1016/j.marpol.2021.104487.

Wernand, M.R., 2010. On the history of the secchi disc. Journal of the European Optical Society: Rapid Publications 5, 10013s. https://doi.org/10.2971/jeos.2010.10013s.

Yang, L., Yu, D., Gai, Y., Gao, H., An, D., Bian, X., Zhou, Y., Liu, X., Tang, S., 2021. Remote sensing retrieval of secchi disk depth in Jiaozhou Bay using Sentinel-2 MSI image. Infrared and Laser Engineering 50 (12), 515–521. https://doi.org/10.3788/IRLA20210080.

Yin, Z., Li, J., Huang, J., Wang, S., Zhang, F., Zhang, B., 2021a. Steady increase in water clarity in Jiaozhou Bay in the Yellow Sea from 2000 to 2018: observations from MODIS. Journal of Oceanology and Limnology 39 (3), 800–813. https://doi.org/10.1007/s00343-020-0124-4.

Yin, Z., Li, J., Liu, Y., Xie, Y., Zhang, F., Wang, S., Sun, X., Zhang, B., 2021b. Water clarity changes in Lake taihu over 36 years based on landsat TM and OLI observations. Int. J. Appl. Earth Obs. Geoinf. 102, 102457 https://doi.org/10.1016/j.jag.2021.102457.

Yu, Z., Yang, K., Luo, Y., Yang, Y., 2021. Secchi depth inversion and its temporal and spatial variation analysis—A case study of nine plateau lakes in Yunnan Province of China. Int. J. Appl. Earth Obs. Geoinf. 100, 102344 https://doi.org/10.1016/j.jag.2021.102344.

Yu, W., Zhang, D., Liao, J., Ma, L., Zhu, X., Zhang, W., Hu, W., Ma, Z., Chen, B., 2022. Linking ecosystem services to a coastal bay ecosystem health assessment: a comparative case study between Jiaozhou Bay and Daya Bay. China. Ecological Indicators 135, 108530. https://doi.org/10.1016/j.ecolind.2021.108530.

Yuan, Y., Jalón-Rojas, I., Wang, X.H., 2021. Response of water-exchange capacity to human interventions in Jiaozhou Bay, China. Estuar. Coast. Shelf Sci. 249, 107088 https://doi.org/10.1016/j.ecss.2020.107088.

Zhang, Y., Shi, K., Zhang, Y., Moreno-Madrinan, M., Xu, X., Zhou, Y., Qin, B., Zhu, G., Jeppesen, E., 2021a. Water clarity response to climate warming and wetting of the Inner Mongolia-Xinjiang plateau: a remote sensing approach. Sci. Total Environ. 796, 148916 https://doi.org/10.1016/j.scitotenv.2021.148916.

Zhang, Y., Zhang, Y., Shi, K., Zhou, Y., Li, N., 2021b. Remote sensing estimation of water clarity for various lakes in China. Water Res. 192, 116844 https://doi.org/10.1016/j.watres.2021.116844.

Zhou, Y., Yu, D., Yang, Q., Pan, S., Gai, Y., Cheng, W., Liu, X., Tang, S., 2021. Variations of water transparency and impact factors in the bohai and yellow seas from satellite observations. Remote Sens. 13 (3), 514. https://doi.org/10.3390/rs13030514.

Zhou, Y., Yu, D., Cheng, W., Gai, Y., Yao, H., Yang, L., Pan, S., 2022. Monitoring multi-temporal and spatial variations of water transparency in the Jiaozhou Bay using GOCI data. Mar. Pollut. Bull. 180, 113815 https://doi.org/10.1016/j.marpolbul.2022.113815.

Zolfaghari, K., Duguay, C., 2016. Estimation of water quality parameters in Lake Erie from MERIS using linear mixed effect models. Remote Sens. 8 (6), 473. https://doi.org/10.3390/rs8060473.